GANIT

GANIT: Journal of Bangladesh Mathematical Society

GANIT*J. Bangladesh Math. Soc.* 46.3 (2026) 015–029
DOI: https://doi.org/10.3329/ganit.v46i01.89270

MHD Darchy-Forchheimer Convective Flow above a Vertical Permeable Plate with Radiative Heat Transfer and Chemical Reaction

Md. Jarif Mollah[a], M. M. Touhid Hossain[a,*]

[a]Department of Mathematics, Khulna University of Engineering & Technology, Khulna-9203, Bangladesh

ABSTRACT

This research investigates two-dimensional, steady-state magnetohydrodynamic (MHD) Darcy-Forchheimer flow over a moving vertical permeable surface within a porous medium. The study considers a laminar convective heat-generating fluid subjected to thermal radiation and chemical reaction effects. By accounting for inertia effects, numerical simulations were performed to analyze how velocity, thermal, and concentration boundary layers respond to various physical parameters under a transverse magnetic field. The governing nonlinear PDEs—representing continuity, momentum, energy, and species concentration—were transformed into a system of ODEs using similarity transformations under the Boussinesq approximation. These equations were subsequently solved using the shooting method (ode45) and the MATLAB BVP4C solver. It is found that, the dimensionless velocity increased by approximately 10.80% as the local Darcy number (Da_x) rose from 0.5 to 5. Conversely, velocity decreased by roughly 5.17% with an increase in the local Forchheimer number (Fc_x) from 0.1 to 1.4, and by 69.38% as the Hartmann number (Ha_x) increased from 0.1 to 5. Thermal performance weakened by 5.72% when Da_x increased and by 45.45% as the radiation parameter (R) rose from 0.1 to 5.0. Furthermore, solute concentration fell by nearly 54.75% due to an increase in the chemical reaction parameter (Kr_x) from 0.2 to 5. While the skin friction coefficient (C_f) declined with higher Darcy numbers, it rose significantly with intensified Lorentz forces (Ha_x) and inertial resistance (Fc_x). Additionally, the local Nusselt number (Nu_x) showed a marked decrease as R intensified, whereas the local Sherwood number (Sh_x) was substantially enhanced by stronger chemical reactions (Kr_x).

Received: November 09, 2025 **Accepted:** April 07, 2026 **Published Online:** June 15,2026

Keywords: MHD; Darcy-Forchheimer flow; permeable plate; radiation; chemical reaction

AMS Subject Classifications 2026: 65L10, 76S05, 76R10, 76W05, 80A20.

*Corresponding Author. *Email Address:* mthosain@math.kuet.ac.bd

1. Introduction

An important research area of fluid dynamics is involved with the study of steady MHD Darcy-Forchheimer

flow over a moving vertical permeable plate, and nowadays, impetus is paid to such types of research through combining the conjugate effects of thermal radiation and chemical reaction. In modern engineering and technologies, it has wide-ranging applications, for instance, in geophysical energy systems, geothermal engineering, and the design of nuclear reactors, thermal radiators and heat exchangers, etc. Besides, the concept of flow through porous medium appears to be playing a paramount role in the variety of scientific domains of applied and engineering research, such as filtration, reservoir engineering, geosciences, biology and biophysics, material science, mechanics, etc.

The simple linear relationship between pressure drops and rate of flow across the porous medium is governed by a law postulated by Darcy (1856), called Darcy's empirical flow model or Darcy's law. This law states that a fluid flow rate is directly proportional to the pressure gradient, and it is shown to be precise only for a slow-moving fluid through a permeable medium. In this flow model, it is considered that the Reynolds number *Re* is sufficiently low, so that the viscous force is dominant over the inertial force in porous media and hence, inertial effects are neglected. However, high flow rates beyond the assumed laminar flow regime can occur in most common phenomena, such as petroleum engineering. Therefore, it is imperative to take into account the high flow rate effect in the flow model of reservoir engineering. In 1901, a Dutch engineer, Philippe Forchheimer, discovered that the relationship between flow rate and potential gradient is non-linear at a sufficiently high velocity, and this non-linearity is increased with flow rate, which is due to inertial effects in porous media. Thus, in porous media and fractures, high velocity flow is modeled by the Forchheimer equation, in which the non-Darcy pressure drop is quadratic in the mass flux. This flow regime corresponds with the higher values of Reynolds numbers. Therefore, at higher flow rates, Darcy's law is usually replaced by the Forchheimer equation, where a term that is quadratic in the flow rate is included in the momentum equation. It is revealed that a substantial research interest in flow through porous media has grown exponentially in recent years. Emphasis is given on uniform-density flow, but inertia effects are under investigation. As a result, day by day, the desire of people to research in this field is increasing. Therefore, the Darcy-Forchheimer model is perhaps the most often used adjustment for Darcian flow with similarity inertia effects. The inertia effect is addressed by including a quadratic velocity factor in the momentum equation and is termed Forchheimer's extension. Thus, Darcy's law, which accounts for the inertial effects (non-linear drag), plays a significant role for high-speed flow velocities through porous media, where the supplement of Forchheimer is indispensable for accurately modeling flows of significantly very high Reynolds numbers.

[1] investigated the fluctuating natural convection flows driven by an oscillating surface temperature from a horizontal circular cylinder. Using the appropriate similarity transformation and employing the Keller box numerical method, the results for the fluctuating flow and temperature distributions were examined in terms of amplitude and phase of local shear stress and surface heat flux coefficients with the effect of pertinent physical parameters. Further, [2] executed the stream-function and the free variable formulations to solve numerically the two two-dimensional steady state problem of natural convection flow past a cylinder of elliptic cross section using the methods of finite difference and Keller-box eliminations.

[3] carried out a two-dimensional analysis of laminar boundary layer flow of viscous incompressible fluid past a thin flat plate using simple phenomenological models. They solved the transformed Blasius boundary layer equation through numerical integration, employing three numerical methods, namely, Nachtsheim-Swigert, Non-linear shooting iteration technique together with sixth order Runge-Kutta-Butcher initial value solver and made a comparison among the results. Adopting the implicit finite difference method, [4] solved the two-dimensional boundary-layer problem of laminar mixed convection flow past a symmetric semi-infinite wedge considering variable thermal surface conditions. The obtained results were verified with the analytical solution for small period and for large time approach of steady state asymptotic solution. They observed that the Prandtl number and mixed convection parameter decreased significantly with varying pressure gradient for a small-time variance.

In recent years, there has been a growing interest in studying the combined application of MHD convective

flow and porous media. Since the heat generation-absorption process is influenced by the use of a magnetic field in electrically conducting fluid flows, in many metallurgical processes, the rate of cooling, and consequently, the desired properties of the finished product, can be controlled through the application of a magnetic field. The use of a transversely applied magnetic field (MHD) creates a Lorentz force that acts on electrically conducting fluid, influencing its velocity and concentration profiles as well as the thermal characteristics of the fluid. The consolidated effects of forced and free convection, which are due to the motion of a moving vertical permeable plate and buoyancy forces, respectively, have brought about its application in geothermal energy recovery, oil extraction and thermal insulation. [5] considered an unsteady mixed convective heat and mass transfer flow past a semi-infinite vertical plate embedded in a uniform porous medium where the plate was moved with a constant velocity in the flow direction in the presence of a transverse magnetic field. [6] explored a study on MHD boundary layer flow in the presence of heat and mass transfer across a vertical plate that is moving in a magnetic field with convective heat transfer at the surface with the external environment. [7] obtained an exact solution for an unsteady two-dimensional MHD natural convection flow of incompressible viscous fluid over a flat plate embedded in a porous medium with wall transpiration. [8] analyzed MHD fluid flow over a vertical porous plate with the assistance of heat generation and thermal radiation. [9] considered the two-dimensional, laminar, steady, Darcy radiative viscous incompressible second order nanofluid (water based) slip flow over a stretching-shrinking sheet embedded in a saturated non-Darcian porous medium with viscous and Ohmic dissipations in the presence of uniform magnetic field and internal heat generation-absorption. [10] investigated the mixed convective flow of viscous fluids caused by a nonlinear inclined stretching surface.

The convective flow of an electrically conducting fluid with thermal radiation and chemical reaction has gained more attention and importance, on such types of researches in recent times. Heat transfer through thermal radiation is a very critical factor influencing the fluid temperature, which has important implications for applications like high-temperature solar collectors and space technology. Whereas chemical reactions play a pivotal role in chemical engineering processes, where concentration control is a supreme interest. Considering the thermal radiation, a numerical solution is presented by [11] to investigate the impacts of radiation absorption, mass diffusion, chemical reaction, and heat source parameter of a heat-producing fluid passing through a porous plate located vertically, subjected to different suction. In the presence of suction with the influence of first-order homogeneous chemical reaction and thermal radiation of unsteady MHD mixed convection fluid flow across a vertical porous plate immersed in a homogenous porous medium, and flow was elucidated by [12]. [13] analyzed the forced convective flow and heat transfer of an incompressible fluid past a plate embedded in a Darcy-Forchheimer porous medium. An investigation was carried out to investigate the effect of thermal radiation and chemical reaction of steady MHD flow across a vertical porous plate, including heat and mass transfer by [14]. [15] presented a time-dependent nonlinear MHD flow of viscous, incompressible, electrically conducting fluid past a vertical permeable channel subject to the impact of thermal radiation and chemical reaction. Further, [16] inspected the MHD and buoyancy effects on convective heat and mass transfer flow past a moving vertical permeable plate with the presence of thermal radiation and chemical reaction. A theoretical analysis of time-dependent flow of blood through a stretching permeable vessel with the impact of magnetic field intensity, together with the thermal radiation and chemical reaction, was accomplished by [17].

Furthermore, the Darcy-Forchheimer model with the incorporation of radiative heat transfer and chemical reactions for unsteady mixed convective flow above a permeable vertical plate embedded in a porous medium is a very crucial phenomenon that is very ubiquitous in high-temperature industrial processes and many chemical engineering applications. The issue of boundary layer forced convective flow and heat transfer of a two-dimensional incompressible fluid via a plate embedded in a Darcy-Forchheimer porous medium with transverse magnetic field and thermal radiation was researched by [18]. [19] explored the consequences of sloped magnetohydrodynamic viscous fluid flow sustained in a non-Darcy porous medium.

[20] analyzed the impact of the squeezing nature of MHD Darcy–Forchheimer nanofluid flow between two horizontal plates.

In the context of the above studies, the steady MHD convective flow for a heat-generating fluid with thermal radiation and chemical reaction has gained more attention, and importance has been given to such type of research in recent years. But addressing the inertia effect, the MHD Darcy-Forchheimer flow via a moving vertical permeable surface is not considered so far, where the combined effects of thermal radiation and chemical reaction were not noticed. Therefore, in the current study, a numerical investigation of two-dimensional steady laminar convective Darcy-Forchheimer flow with heat and mass transfer past a moving vertical permeable plate in a porous medium is carried out, consolidating both the impacts of thermal radiation and chemical reaction subjected to the effects of inertial resistance and transverse magnetic field. Adopting the method of similarity transformations under the assumption of the Boussinesq approximation, the numerical calculations are performed with a view to studying the velocity, temperature and concentration fields. Later, a parametric study has been carried out to explore the effect of some important pertinent dimensionless parameters, namely, Darcy number (Da_x), Forchheimer number (Fc_x), Hartmann number (Ha_x), Thermal radiation parameter (R) and Chemical reaction parameter (Kr_x). The effects of these parameters on skin-friction coefficient (C_f), the local Nusselt number (Nu_x) and the local Sherwood number (Sh_x) have also been discussed.

2. Formulation of the Problem

For a steady-state flow condition in which the flow rate across the outer boundary of a given volume is the same as the flow rate across the inner boundary, the flow speed u is related to the pressure gradient according to Dercy's law as:

$$-\frac{\partial p}{\partial x} = \frac{\mu}{k'}u \tag{2.1}$$

where k' is specific permeability (m^2) of the medium.

To extend applicability for high flow rate, that is, for higher Reynolds number (Re), a quadratic term is arbitrarily added, resulting in the 'Forchheimer Law':

$$-\frac{\partial p}{\partial x} = \frac{\mu}{k'}u + \frac{\rho C^*}{\sqrt{k'}}u^2 \tag{2.2}$$

where C^* is the drag force coefficient (m^2) of the medium.

Let us consider a boundary layer steady two-dimensional flow including heat transfer over a moving vertical permeable plate in an incompressible electrically conducting fluid possessing chemical reaction and heat source. Suppose that the left surface of the plate is being heated through convection from hot fluid at temperature T_f, where the convection heat transfer coefficient is h_f and the fluid temperature away from the plate is T_∞. Let the x-axis be taken along the plate direction, whereas the y-axis is normal to it. A uniform magnetic field of strength B_0 is applied normally from the negative direction of the y-axis, that produced magnetic effects in the direction of the x-axis. The magnetic Reynolds number is assumed very small so that the induced magnetic field effects can be ignored. The components velocity in the x- and y-directions, temperature and concentration are denoted by the symbols u, v, T and C, respectively. The physical flow model and the coordinate system are shown in Fig. 2.1.

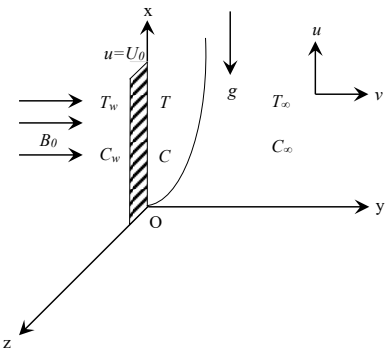

Fig. 2. 1. The flow model and coordinate system

Then the governing equations for a Darcy-Forchheimer flow involving the continuity, momentum, energy, and mass concentration under the Boussinesq approximation can be expressed as follows:

$$\frac{\partial u}{\partial x}+\frac{\partial v}{\partial y}=0 \tag{2.3}$$

$$u\frac{\partial u}{\partial x}+v\frac{\partial u}{\partial y}=\upsilon\frac{\partial^2 u}{\partial y^2}-\frac{\upsilon}{k'}u-\beta' u^2-\frac{\sigma B_0^2 u}{\rho}+g\beta(T-T_\infty)+g\beta^*(C-C_\infty) \tag{2.4}$$

$$u\frac{\partial T}{\partial x}+v\frac{\partial T}{\partial y}=\frac{k}{\rho C_P}\frac{\partial^2 T}{\partial y^2}+\frac{Q_0}{\rho C_P}(T-T_\infty)-\frac{1}{\rho C_P}\frac{\partial q_r}{\partial y} \tag{2.5}$$

$$u\frac{\partial C}{\partial x}+v\frac{\partial C}{\partial y}=D\frac{\partial^2 C}{\partial y^2}-K_r'(C-C_\infty) \tag{2.6}$$

The corresponding boundary conditions for the problem are –

$$u=U_0,\ v=v_0,\ -k\frac{\partial T}{\partial y}=h_f(T_f-T),\ C=\ C_w \text{ at } y=0 \tag{2.7}$$

$$u=0, T=T_\infty,\ C=C_\infty \text{ at } y\to\infty \tag{2.8}$$

where υ = kinematic viscosity, β = thermal expansion coefficient, β^* = solutal expansion coefficient, $\beta'=C^*/\sqrt{k'}$ is the inertial coefficient, ρ = fluid density, g = gravitational acceleration, σ = electrical conductivity, Q_0 = volumetric rate of heat generated from an internal heat source, C_p = specific heat at constant pressure, D = mass diffusivity, K_r' = chemical reaction rate on the species concentration, C_w = species concentration at the plate surface, U_0 = plate velocity, v_0 = suction velocity of the wall, k = thermal conductivity coefficient, k' = permeability of the medium, and C_∞ = concentration of the fluid away from the plate.

The physical parameters of interest are the local Nusselt number Nu_x, skin friction (fanning friction factor) C_f and local Sherwood number Sh_x, which are defined by:

$Nu_x=\frac{xq_w}{k(T_w-T_\infty)}$, $C_f=\frac{\tau_w}{\frac{1}{2}\rho u_\infty^2}$ and $Sh_x=\frac{xk_c}{D(C_w-C_\infty)}$, where $q_w=-k\left(\frac{\partial T}{\partial y}\right)_{y=0}$ represents the wall heat flux, $\tau_w=\mu\left(\frac{\partial u}{\partial y}\right)_{y=0}$ represents the wall shear stress and $k_c=-D\left(\frac{\partial C}{\partial y}\right)_{y=0}$ is the wall mass transfer rate and u_∞ is the velocity of the bulk fluid (Free-stream velocity).

As the governing boundary layer equations (2.3) to (2.6) given above, together with boundary conditions (2.7) and (2.8), are coupled and purely nonlinear, the evaluation of the exact solution of the system of equations is quite cumbersome. Therefore, the following similarity transformations are introduced to those nonlinear partial differential equations to convert them in a set of ordinary differential equations:

$$\eta=y\sqrt{\frac{U_0}{\nu x}},\ u=U_0 f'(\eta),\ v=-\frac{1}{2}\sqrt{\frac{\nu U_0}{x}}f(\eta)+\frac{U_0 y}{2x}f'(\eta),\ \theta(\eta)=\frac{T-T_\infty}{T_f-T_\infty} \text{ and } \phi(\eta)=\frac{C-C_\infty}{C_w-C_\infty} \tag{2.9}$$

where prime represents the differentiation with respect to η. Let's discuss the dimensionless quantities, which are

$$Da_x = \frac{k'}{x^2}, Fc_x = \frac{k'\beta'}{x}, \ Re_x = \frac{U_0 x}{\nu}, \ Ha_x = \frac{\sigma B_0^2 x}{\rho U_0} \ Gr_x = \frac{g\beta(T_f - T_\infty)x}{U_0^2}, Gm_x = \frac{g\beta^*(C_w - C_\infty)x}{U_0^2}, \quad S_x = \frac{Q_0 x}{\rho C_P U_0},$$
$$Sc = \frac{\nu}{D}, \ BI_x = \frac{h_f}{k}\sqrt{\frac{\nu x}{U_0}}, \Pr = \frac{\mu C_P}{k}, R = \frac{4\sigma_1 T_\infty^3}{K_1 U_0}, \lambda = \frac{k}{U_0}, Kr_x = \frac{Kr' x}{U_0} \tag{2.10}$$

Here Da_x it the local Darcy number, Fc_x is the local Forchheimer number, Re_x is the local Reynolds number, Ha_x is the local magnetic field parameter or local Hartman number, Gr_x is the local thermal Grashof number, Gm_x is the local solute Grashof number, S_x is the local heat source parameter, BI_x is the local convective heat source parameter and Kr_x is the local chemical reaction parameter, which are all functions x and are produced locally from the similarity solution. Also, it is considered that the Schmidt number is Sc, the Prandtl number is Pr, the thermal radiation parameter is Re, the Stefan-Boltzmaan constant is σ, the mean absorption coefficient is K_1, and λ is a scaling factor. Now using (2.9) and (2.10) in (2.4) - (2.6), we get the following equations:

$$f''' + \frac{1}{2}ff'' - \left(Ha_x + \frac{1}{Da_x Re_x}\right)f' - \frac{Fc_x}{Da_x}f'^2 + Gr_x\theta + Gm_x\varphi = 0 \tag{2.11}$$

$$\left(1 + \frac{4}{3}\frac{R}{\lambda}\right)\theta'' + \frac{1}{2}\Pr f\theta' + s_x \Pr \theta = 0 \tag{2.12}$$

$$\varphi'' + \left(\frac{1}{2}f - Kr_x\right)Sc\varphi = 0 \tag{2.13}$$

$$f(0) = 0, f'(0) = 1, \theta'(0) = BI_x\{\theta(0) - 1\}, \varphi(0) = 1, f'(\infty) = 0, \theta(\infty) = 0, \varphi(\infty) = 0 \tag{2.14}$$

For a perfect similarity solution, it is assumed that $k' = ax^2$, $\beta' = bx^{-1}$, $\sigma = cx^{-1}$, $h_f = dx^{-\frac{1}{2}}$, $\beta = ex^{-1}$, $\beta^* = mx^{-1}$, $Q_0 = nx^{-1}$, and $Kr' = qx^{-1}$, where a, b, c, d, e, m, n and q are constants having proper dimensions. Furthermore, the physical quantities of interest, namely, local Nusselt number Nu_x, skin friction (fanning friction factor) C_f and local Sherwood number Sh_x in non-dimensional forms are now proportional to $f''(0)$, $-\theta'(0)$, and $-\varphi'(0)$, respectively.

3. Numerical Methodology

The reformed similarity equations (2.11) – (2.13), along with initial and boundary conditions (2.14), are solved numerically using the shooting method and the bvp4c procedure in 'MATLAB'. The bvp4c is a dedicated BVP solver that utilized a global collocation method to solve more complex problem. In contrast, he shooting method is an iterative, trial-and-error process typically employs the ode45 solver to treat BVPs. It accomplishes this by reformulating the BVPs as a series of IVPs and solving them through integration. Since ode45 can only solve first-order systems. Any higher order BVPs must first be converted into a first-order system of equations by defining new variables, such as, $y_1 = y$, $y_2 = y'$, and so on. A root finding algorithm is used to refine the guesses for the unknown values until the residual at the boundary is minimized to approximately zero. For this specific problem, the relative and absolute error tolerances are set to $1e^{-8}$.

4. Numerical Results and Discussion

The numerical simulations were conducted to examine how the velocity, temperature and concentration distributions vary across several key dimensionless parameter/number. To isolate the influence of a specific parameters/numbers on the velocity, temperature and concentration profiles, a "one-at-a-time" sensitivity approach was employed in the numerical procedure, where all other parameters/numbers remained constant. The baseline values of the parameter/number assigned for this procedure are: $Ha_x = 0.1$, $Da_x = 5.0$, $Re_x = 5.0$, $Fc_x = 0.1$, $Gr_x = 0.1$, $Gm_x = 0.1$, $Pr = 5.0$, $R = 0.5$, $S_x = 0.1$, $Sc = 0.78$, $Kr_x = 3.0$, $BI_x = 1.0$ and $\lambda = 0.6$. This systematic analysis provides a deeper physical insight into the transport phenomena involved in the problem.

4.1. Variation of Darcy Number (Da_x)

Figs. 4.1.1– 4.1.2 convey the velocity, temperature and concentration profiles as the local Darcy number (Da_x) varies between 0.5 to 5.0. Since Da_x represents the ratio of the medium's permeability (k') to the square of the characteristic length scale (x), a high value of Da_x indicates that the porous medium is highly permeable relative to the flow domain. Conversely, a low Da_x suggests significant flow resistance leading to highly

confined fluid motion. As Da_x increases- and consequently, the permeability of the medium rises- the improved fluid penetration into the permeable structure results in a reduction of overall flow resistance (drag force). This reduction facilitates a boost in momentum transfer, leading to the higher velocities observed in

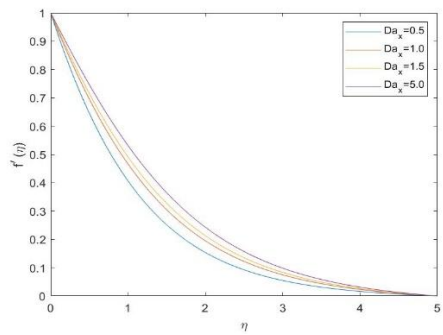

Fig. 4.1.1. Variation of velocity ($f'(\eta)$) with local Darcy number (Da_x)

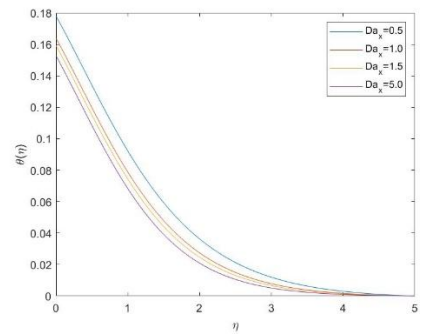

Fig. 4.1.2. Variation of temperature ($\theta(\eta)$) with local Darcy number (Da_x)

Fig. 4.1.1. These results confirm the physical role of the Darcy number as a parameter representing resistance to flow. Fig. 4.1.2 depicts the variation of the temperature profile with respect to Da_x. As Da_x increases, the temperature at any given position decreases and asymptotically approaches zero. Because higher Da_x values correspond to lower flow resistance, the fluid can move at higher velocities, enabling more heat convection away from the heated surface efficient Consequently, increasing Da_x accelerates heat transfer, which thins the thermal boundary layer and lowers the fluid temperature. Finally, Fig. 4.1.3 examines the impact of Da_x on the concentration component. The results show that the concentration profile $\phi(\eta)$ starts at unity and rapidly decays toward zero for large values of η across all Da_x values. Notably, the Darcy number appears to have no significant influence on the concentration distribution.

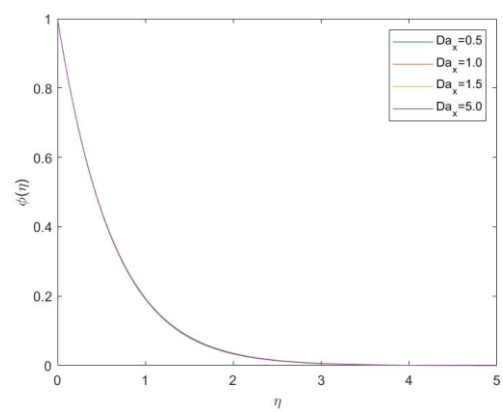

Fig. 4.1.3. Variation of concentration ($\varphi(\eta)$) with local Darcy number (Da_x)

4.2. Variation of Forchheimer Number (Fc_x)

Fig. 4.2.1 illustrates the variation in velocity profiles against the similarity variable η for various values of the local Forchheimer number (Fc_x). As shown, an increase in Fc_x (from 0.1 to 1.4) results in a reduction of the velocity ($f'(\eta)$) throughout the boundary layer, leading to a thinner velocity boundary layer.

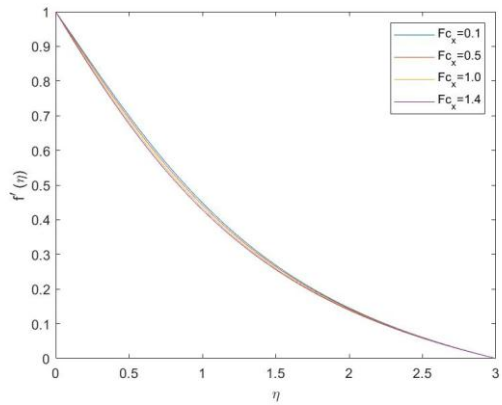

Fig. 4.2.1. Variation of velocity ($f'(\eta)$) with local Forchheimer number (Fc_x)

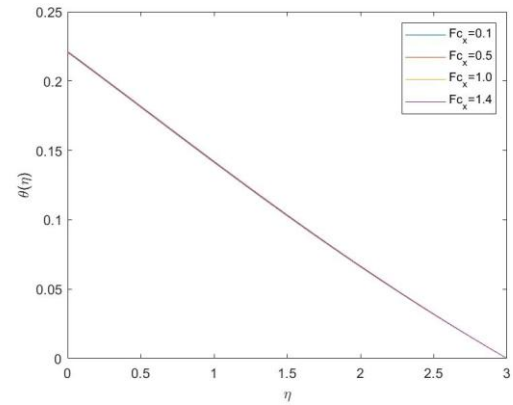

Fig. 4.2.2. Variation of temperature ($\theta(\eta)$) with local Forchheimer number (Fc_x)

Because Fc_x accounts for non-linear inertial effects (β') that deviate from the linear Darcy's law, it becomes particularly significant at higher flow velocities. Rising Fc_x values intensify these inertial effects, thereby increasing the inertial drag force exerted by the porous medium. This enhanced resistance retards fluid motion and decreases velocity across the entire boundary layer. Conversely, Fc_x exerts a negligible influence on temperature and concentration distributions. As observed in Figs. 4.2.2 and 4.2.3, both temperature and concentration profiles decay sharply as η increases, asymptotically converging to zero for large values of the similarity variable.

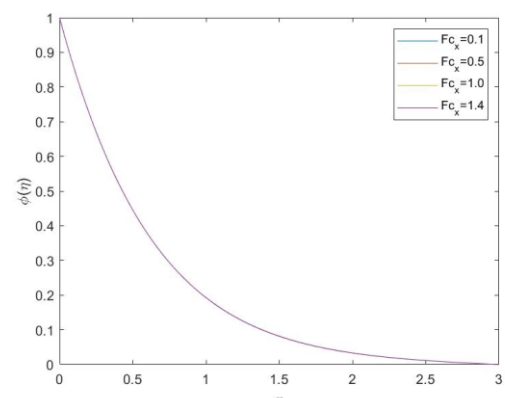

Fig. 4.2.3. Variation of concentration ($\varphi(\eta)$) with local Forchheimer number (Fc_x)

4.3. Variation of Hartmann Number (Ha_x)

Figs. 4.3.1– 4.3.3 demonstrate the impact of various local Hartmann numbers (Ha_x) on the velocity, thermal, and concentration profiles relative to the similarity variable η. Since the Hartmann number represents the ratio of electromagnetic drag (the Lorentz force) to viscous force within the boundary layer, higher Hax values indicate a more potent applied magnetic field (B_0) or enhanced electrical conductivity (σ). This intensification produces a robust resistive force within the electrically conducting fluid. As illustrated in Fig. 4.3.1, this retarding effect thickens the momentum boundary layer and subsequently decelerates the fluid velocity across the entire region.

Fig. 4.3.2 illustrates the response of the temperature field to changes in the local Hartmann number (Ha_x). The data indicates that at a specific location, the dimensionless temperature ($\theta(\eta)$) rises in correlation with Ha_x. This thermal elevation suggests that intensifying the magnetic field strength enhances the internal temperature of the fluid. This phenomenon is attributed to the augmentation of Joule heating when an external magnetic field interacts with an electrically conducting fluid. Furthermore, the increased frictional resistance induced by a potent magnetic field generates additional heat. Consequently, the bulk fluid temperature rises, leading to an expansion of the thermal boundary layer thickness. Furthermore, Fig. 4.3.3 depicts the variation in concentration ($\varphi(\eta)$) relative to Ha_x. It is evident that as Ha_x increases from 0.1 to 5.0, the concentration field within the boundary layer slightly rises, which corresponds to an increase in the concentration boundary layer thickness. Strengthening the magnetic field intensifies the Lorentz force, acting as a resistive body force against the fluid motion. Given that the concentration field is inversely linked to the velocity field, this retarding effect suppresses mass transport away from the surface. Consequently, the concentration within the boundary layer increases, resulting in a broader concentration profile. Ultimately, these results confirm that the application of a magnetic field serves as an effective mechanism for regulating flow, temperature, and concentration distributions.

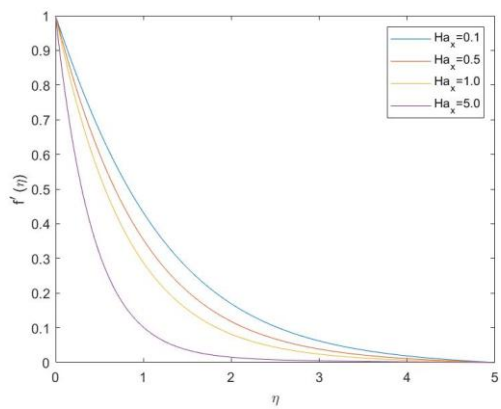

Fig. 4.3.1. Variation of velocity ($f'(\eta)$) with local magnetic field parameter (Ha_x)

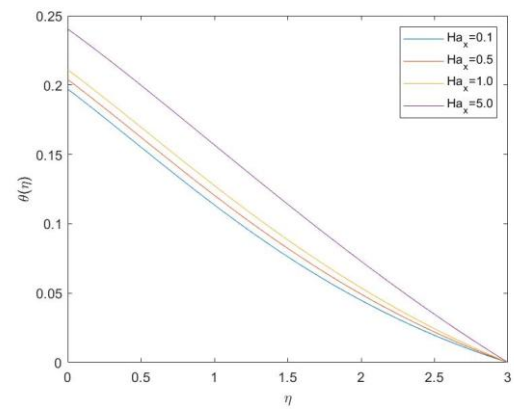

Fig. 4.3.2. Variation of temperature ($\theta(\eta)$) with local magnetic field parameter (Ha_x)

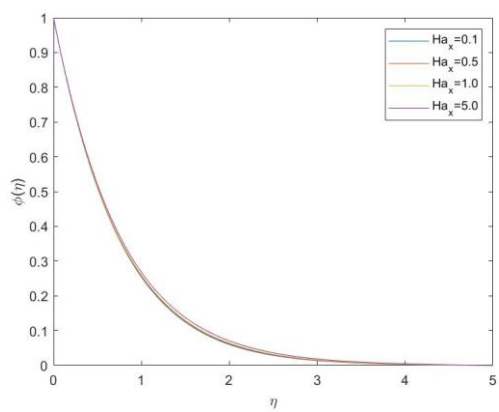

Fig. 4.3.3. Variation of concentration ($\varphi(\eta)$) with local magnetic field parameter (Ha_x)

4.4. Variation of Thermal Radiation Parameter (R)

Fig. 4.4.1 interprets the velocity variations relative to the similarity variable \eta as a function of the local thermal radiation parameter (R). In this study of Forchheimer flow over a stretching sheet, the dimensionless velocity is found to decrease for $\eta > 0$ as R increases from 0.1 to 5.0, which is attributed to an increase in the boundary layer thickness. Similarly, Fig. 4.4.2 illustrates the temperature curves for various values of R. As the radiation parameter rises, the temperature profiles decline across the entire boundary layer. This cooling effect becomes more pronounced at higher R values, suggesting that thermal radiation is an effective mechanism for enhancing cooling performance.

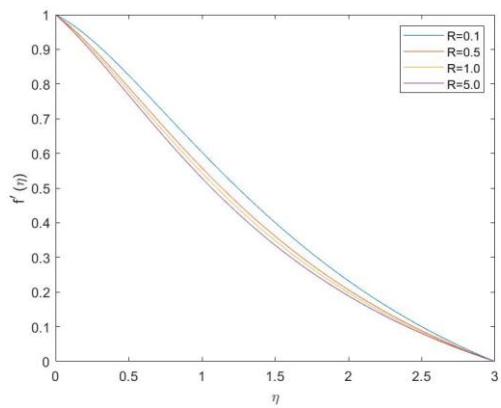

Fig. 4.4.1. Variation of velocity ($f'(\eta)$) with local thermal radiation parameter (R)

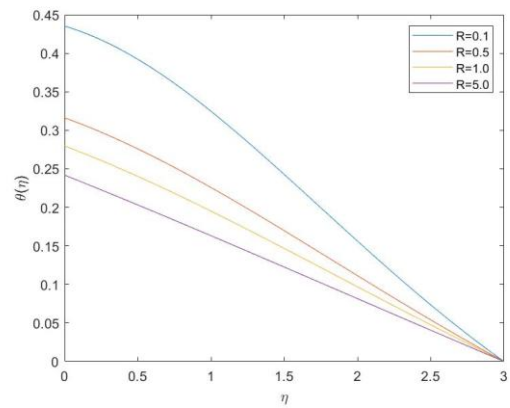

Fig. 4.4.2. Variation of temperature ($\theta(\eta)$) with local thermal radiation parameter (R)

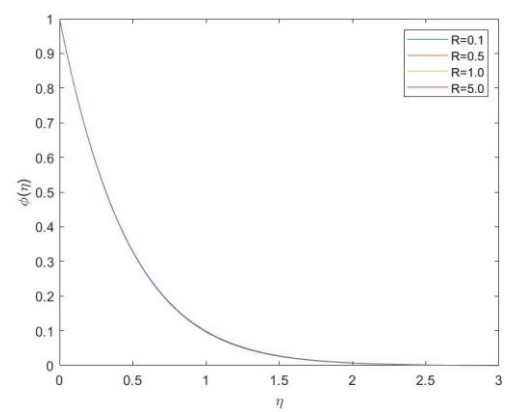

Fig. 4.4.3. Variation of concentration ($\varphi(\eta)$) with local thermal radiation parameter (R)

In contrast, Fig. 4.4.3 indicates that the concentration field remains largely unaffected by variations in R; however, the concentration profiles follow the expected trend of decreasing as the non-dimensional distance η from the surface increases.

4.5. Variation of Chemical Reaction Parameter (Kr_x)

Fig. 4.5.1 displays the velocity variation in relation to the local chemical reaction parameter (Kr_x). It is observed that Kr_x exerts a marginal influence on fluid velocity; as Kr_x increases from 0.2 to 5.0, the velocity profiles exhibit a slight reduction across the boundary layer. When an increase in Kr_x initiates an endothermic reaction, it diminishes the thermal and solutal buoyancy driving forces. This results in heightened viscous resistance, which retards fluid motion and subsequently lowers the velocity profile. Consequently, higher Kr_x values lead to increased frictional forces, causing a decline in fluid velocity. Correspondingly, Fig. 4.5.2 presents the temperature variation against the similarity variable η for varying Kr_x. In contrast to the velocity field, the temperature increases slightly as Kr_x rises from 0.2 to 5.0. This elevation suggests that the chemical reaction within the fluid domain facilitates internal heat generation. The energy released at a higher reaction rate adds thermal energy to the system, resulting in a warmer fluid environment compared to cases with lower chemical reaction rates.

Fig. 4.5.3 explores the concentration field relative to η for various values of the local chemical reaction parameter (Kr_x). It is evident that Kr_x significantly impacts the concentration field; a marked reduction in the concentration curve is observed across the boundary layer as Kr_x increases. Since Kr_x represents the ratio of the chemical reaction rate to the convective transport rate, higher values lead to a substantial thinning of the concentration boundary layer. This promotes a higher mass transfer rate, as rapid chemical consumption induces a steeper concentration gradient at the surface.

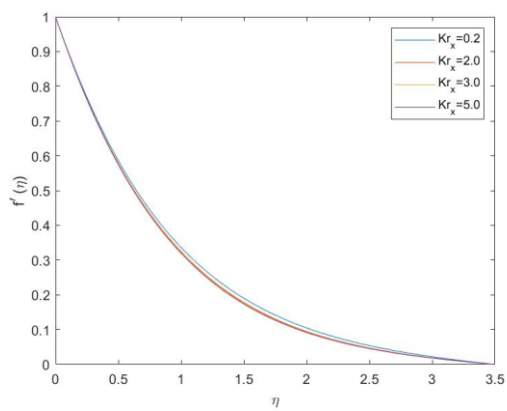

Fig. 4.5.1. Variation of velocity ($f'(\eta)$) with local chemical reaction parameter (Kr_x)

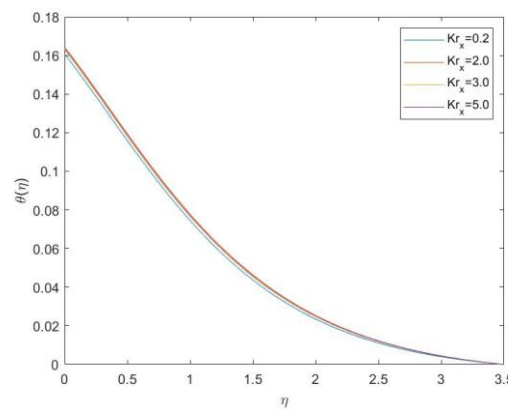

Fig. 4.5.2. Variation of temperature ($\theta(\eta)$) with local chemical reaction parameter (Kr_x)

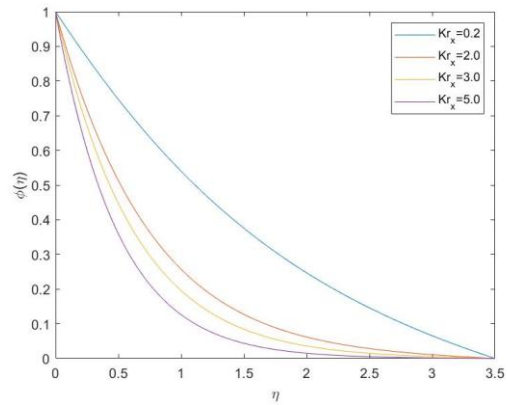

Fig. 4.5.3. Variation of concentration ($\boldsymbol{\varphi(\eta)}$) with local chemical reaction parameter (Kr_x)

4.6. Variation of Local skin friction coefficient (C_f), Nusselt number (Nu_x) and Sherwood number (Sh_x)

Based on the numerical computation process, values for $f''(0)$, $-\theta'(0)$, and $-\varphi'(0)$ were determined. These quantities are directly proportional to the local skin friction coefficient (C_f), the Nusselt number (Nu_x), and the Sherwood number (Sh_x), respectively. These physical parameters of interest are presented in Table 4.6.1.

Table 4.6.1 illustrates how various non-dimensional parameters influence skin friction (C_f), the Nusselt number (Nu_x), and the Sherwood number (Sh_x). These physical quantities are proportional to the velocity gradient at the wall ($f''(0)$), the surface heat transfer rate ($-\theta'(0)$), and the mass transfer rate ($-\varphi'(0)$), respectively. Because $f''(0)$, represents shear stress, an increase in its magnitude (becoming more negative) indicates higher skin friction.

Table 4.6.1: Computation of numerical results presenting the values of $f''(0)$, $\theta'(0)$, and $\varphi'(0)$ for various pertinent parameters

Da_x	Fc_x	Ha_x	R	Kr_x	$f''(0)$	$-\theta'(0)$	$-\varphi'(0)$
0.5	0.1	0.1	0.5	3.0	-0.65	0.083	0.75
1.0	0.1	0.1	0.5	3.0	-0.55	0.082	0.80
5.0	**0.1**	0.1	0.5	3.0	-0.42	0.073	0.90
5.0	**1.0**	0.1	0.5	3.0	-0.48	0.073	1.21
5.0	**1.4**	0.1	0.5	3.0	-0.50	0.073	1.30
5.0	0.1	**0.1**	0.5	3.0	-0.42	0.073	0.90
5.0	0.1	**1.0**	0.5	3.0	-1.30	0.077	0.98
5.0	0.1	**5.0**	0.5	3.0	-2.50	0.080	1.00
5.0	0.1	0.1	**0.1**	3.0	-0.32	0.140	0.90
5.0	0.1	0.1	**0.5**	3.0	-0.42	0.073	0.90
5.0	0.1	0.1	**5.0**	3.0	-0.48	0.070	0.90
5.0	0.1	0.1	0.5	**0.2**	-0.40	0.064	0.45
5.0	0.1	0.1	0.5	**3.0**	-0.42	0.073	0.90
5.0	0.1	0.1	0.5	**5.0**	-0.50	0.075	1.15

Observations show that as the Darcy number (Da_x) rises from 0.5 to 5.0, $f''(0)$ increases from -0.65 to -0.42. This shift toward zero signifies reduced skin friction, likely due to enhanced wall permeability. Conversely, increasing the Forchheimer number (Fc_x) makes $f''(0)$ more negative, suggesting that inertial resistance intensifies skin friction. A more pronounced effect is seen with the Hartmann number (Ha_x), where $f''(0)$, drops sharply from -0.42 to -2.50, confirming that the Lorentz force significantly boosts surface shear stress. Regarding thermal dynamics, the Radiation parameter (R) exerts the most substantial influence. As R increases from 0.1 to 5.0, ($-\theta'(0)$), decreases markedly, implying that heightened thermal radiation thickens the thermal boundary layer and inhibits the heat transfer rate at the wall. However, rising Ha_x and Chemical reaction (Kr_x) values slightly enhance heat transfer. Furthermore, as Kr_x scales from 0.2 to 5.0, the mass

transfer rate ($-\varphi'(0)$) increases substantially. This indicates that chemical reactions act as a primary driver for mass transport. Similarly, higher Da_x and Fc_x values lead to marginal gains in mass transfer. These quantitative findings align with the results established by [6] for a Prandtl number (Pr) of 7.1.

5. Conclusion

Based on the current investigation, the following conclusions have been established:

(i) Influence of Inertia: The non-Darcy term, representing inertial effects and quantified by the Forchheimer number (Fc_x), exerts a substantial retarding effect on the flow field he non-Dercian term related to the inertial effect which is quantified by the Forchheimer number (Fc_x) has a very significant influence on decreasing the flow field.

(ii) Magnetohydrodynamic Effects: An increase in the magnetic parameter, expressed via the Hartmann number (Ha_x), causes a reduction in fluid velocity; conversely, it enhances the temperature distribution within the field.

(iii) Thermal Radiation: Elevated levels of the local thermal radiation parameter (R) serve to suppress both the velocity and temperature profiles.

(iv) Chemical Kinetics: Rising values of the local chemical reaction parameter (Kr_x) lead to a marginal decline in velocity and temperature, while significantly depleting the concentration field.

(v) Surface Friction and Shear Stress: While skin friction diminishes as the Darcy number (Da_x) rises from 0.5 to 5.0, both the Lorentz force (Ha_x) and inertial resistance (Fc_x) notably intensify the wall shear stress.

(vi) Heat Transfer Dynamics: The rate of heat transfer at the wall experiences its most pronounced decrease in response to an increase in the radiation parameter (R).

(vii) Mass Transfer: A more potent chemical reaction (Kr_x) results in a substantial enhancement of the mass transfer rate.

Acknowledgements

This work is a part of the research of M.Sc. degree of the first author so that, he would like to express her gratitude to the Khulna University of Engineering & Technology (KUET), particularly to the Department of Mathematics, KUET for providing all kind of supports including financial assistance to continue his M.Sc. program. The authors are sincerely grateful to the academic reviewers for their insightful comments those were helped to improve the quality of the manuscript.

Funding

A partial funding was received from the Committee for Advanced Studies and Research (CASR) of Khulna University of Engineering & Technology (KUET) as a part of its research publication budget.

Nomenclature

C_p	Specific heat at constant pressure	C_w	Concentration at the plate surface
g	Gravitational acceleration	x, y	Dimensional coordinates
k_c	Wall mass transfer rate	C_∞	Away concentration
k'	Specific permeability of the medium	τ_w	Wall shear stress
C^*	Drag force coefficient of the medium	C_f	Skin friction coefficient
Q_0	Volumetric rate of heat	β	Thermal expansion coefficient
B_0	Magnetic field strength	β^*	Solutal expansion coefficient
h	Local heat transfer coefficient	υ	Kinematic viscosity
D	Mass diffusivity	η	Nondimensional length scale
k	Thermal conductivity	σ	Stefan-Boltzmaan constant
$k^{'}$	Permeability of the medium	ρ	Density
K_1	Mean absorption coefficient	θ	Dimensionless temperature

K_r'	Chemical reaction rate	φ	Dimensionless concentration
p	Dimensional pressure	μ	Dynamic viscosity
q_w	Wall heat flux	λ	Scaling factor
h_f	Convection heat transfer coefficient	BI_x	Local convective heat source parameter
q_r	Radiative heat flux	Nu_x	Local Nusselt number
U_0	Plate velocity	Sh_x	Local Sherwood number
v_0	Suction velocity at the wall	Gr_x	Local thermal Grashof number
u_∞	Bulk fluid velocity	Gm_x	Local solute Grashof number
u, v	Dimensional velocity components	Ha_x	Local Hartman number
f	Dimensionless velocity	Pr	Prandtl number
T	Dimensional temperature	Re_x	Local Reynolds number
T_f	Hot fluid temperature	S_x	Local heat source parameter
T_w	Wall temperature	Da_x	Local Darcy number
T_∞	Away temperature	Fc_x	Local Forchheimer number
C	Dimensional fluid concentration	Kr_x	Local chemical reaction parameter
		a, b, c, d, e, m, n, q	Dimensional constants

References

[1] Hossain, M. A., Kamrujjaman, M., & Gorla, R. S. R. (2009). Fluctuating free convection flow along eated horizontal circular cylinders. International Journal of Fluid Mechanics Research, 36(3), 207–230.
[2] Jaman, M. K., & Hossain, M. A. (2010). Effect of fluctuating surface temperature on natural convection flow over cylinders of elliptic cross section. Open Transport Phenomena Journal, 2(1), 35–47.
[3] Jaman, M. K., Molla, M. R., & Sultana, S. (2011). Numerical approximations of Blasius boundary layer equation. Dhaka University Journal of Science, 59(1), 87–90.
[4] Bhowmick, S., Jaman, M. K., & Khan, M. Z. I. (2011). Two-dimensional unsteady boundary layer flow with mixed convection along a semi-infinite symmetric wedge. Dhaka University Journal of Science, 59(1), 47–54.
[5] Chamkha, A. J. (2004). Unsteady MHD convective heat and mass transfer past a semi-infinite vertical permeable moving plate with heat absorption. International Journal of Engineering Science, 42, 217–230.
[6] Makinde, O. D. (2010). On MHD heat and mass transfer over a moving vertical plate with a convective surface boundary condition. Canadian Journal of Chemical Engineering, 88(6), 983–990.
[7] Abdulhameed, M., Khan, I., & Shafie, S. (2013). Closed form solutions for unsteady MHD flow in a porous medium with wall transpiration. Journal of Porous Media, 16(9), 795–809.
[8] Mangathai, P., Reddy, G. V. R., & Reddy, B. R. (2016). MHD free convective flow past a vertical porous plate in the presence of radiation and heat generation. International Journal of Chemical Sciences, 14(3), 1577–1597.
[9] Ganesh, N. V., Hakeem, A. A., & Ganga, B. (2018). Darcy–Forchheimer flow of hydromagnetic nanofluid over a stretching/shrinking sheet in a thermally stratified porous medium with second-order slip, viscous and Ohmic dissipation effects. Ain Shams Engineering Journal, 9(4), 939–951.
[10] Hayat, T., Haider, F., & Alsaedi, A. (2020). Darcy–Forchheimer flow with nonlinear mixed convection. Applied Mathematics and Mechanics, 41(11), 1685–1696.
[11] Ibrahim, F. S., Elaiw, A. M., & Bakr, A. A. (2008). Effect of chemical reaction and radiation absorption on unsteady MHD free convection flow past a semi-infinite vertical permeable moving plate with heat source and suction. Communications in Nonlinear Science and Numerical Simulation, 13(6), 1056–1066.
[12] Sharma, B. K., Yadav, K., Mishra, N. K., & Chaudhary, R. C. (2012). Soret and Dufour effects on unsteady MHD mixed convection flow past a radiative vertical porous plate embedded in a porous medium with chemical reaction. Applied Mathematics, 3, 717–723.

[13] Mukhopadhyay, S., De, P. R., Bhattacharyya, K., & Layek, G. C. (2012). Forced convective flow and heat transfer over a porous plate in a Darcy–Forchheimer porous medium in presence of radiation. Meccanica, 47, 153–161.
[14] Lakshmi, R., Jayarami, K. R., Ramakrishna, K., & Reddy, G. R. (2014). Numerical solution of MHD flow over a moving vertical porous plate with heat and mass transfer. International Journal of Chemical Sciences, 12(4), 1487–1499.
[15] Malapati, V., & Polarapu, P. (2015). Unsteady MHD free convection heat and mass transfer in a boundary layer flow past a vertical permeable plate with thermal radiation and chemical reaction. Procedia Engineering, 127, 791–799.
[16] Reddy, G. V. R., Reddy, N. B., & Gorla, R. S. R. (2016). Radiation and chemical reaction effects on MHD flow along a moving vertical porous plate. International Journal of Applied Mechanics and Engineering, 21(1), 157–168. https://doi.org/10.1515/ijame-2016-0010
[17] Zigta, B. (2020). Effect of thermal radiation and chemical reaction on MHD flow of blood in a stretching permeable vessel. International Journal of Applied Mechanics and Engineering, 25(3), 198–211.
[18] Jhankal, A. K., Jat, R. N., & Kumar, D. (2017). Magnetohydrodynamics (MHD) forced convective flow and heat transfer over a porous plate in a Darcy–Forchheimer porous medium in presence of radiation. International Journal of Current Research, 9(11), 1663–1674.
[19] Saif, R. S., Muhammad, T., & Sadia, H. (2020). Significance of inclined magnetic field in Darcy–Forchheimer flow with variable porosity and thermal conductivity. Physica A: Statistical Mechanics and Its Applications, 551, 124067.
[20] Rasool, G., Khan, W. A., Bilal, S. M., & Khan, I. (2020). MHD squeezed Darcy–Forchheimer nanofluid flow between two h-distance apart horizontal plates. Open Physics, 18(1), 1100–1107.